


Climatic characteristics of drift ice in the northern Barents Sea

Chenglin Duan, Sheng Dong, Zhifeng Wang  and Zhenkun Liao

ABSTRACT

In this paper, a preliminary climatic description of the long-term offshore drift ice characteristics in the northern Barents Sea has been investigated from 1987 to 2016 based on the satellite ice motion datasets from National Snow and Ice Data Center (NSIDC) and reanalysis ice thickness datasets from National Centers for Environmental Prediction (NCEP)-Climate Forecast System Reanalysis (CFSR) and Climate Forecast System Version 2 (CFSv2). Both the ice velocity and thickness conditions have been studied at the three fixed locations from west to east. Annual and monthly drift ice roses indicate that the directions from WSW to SE are primarily prevailing, particularly in winter months. Besides, the annual ice speed extremums exceeding 40 cm s^{-1} mostly occur in the southerly directions from November to April. For the ice thickness, results reveal that it is prominently distributed in a thicker interval between 70 and 120 cm, and a thinner interval between 20 and 70 cm. The annual thickness maxima approximately range from 90 to 170 cm, primarily occurring from May to June, and demonstrate a light decreasing trend.

Key words | Barents Sea, climatic pattern, drift ice, ice motion, ice thickness, interannual variation

Chenglin Duan
Sheng Dong
Zhifeng Wang  (corresponding author)
Zhenkun Liao
College of Engineering,
Ocean University of China,
Qingdao 266100,
China
E-mail: wzf1984@ouc.edu.cn

INTRODUCTION

Sea ice is a frozen state of water. The extensive sea ice cover can play a key part in the global air-ice-ocean coupling climate system and sea ice characteristics in the Arctic have been attracting great attention in recent years. The Barents Sea is one of the most remarkable ice changing regions in the Arctic. To our knowledge, relevant literature primarily focuses on sea ice concentration anomalies and external influencing factors, such as the ice concentration peculiarities and variations (e.g. Kern *et al.* 2010), the role of inflowing Atlantic warmer waters and atmospheric forcing (Sorteberg & Kvingedal 2006; Nakanowatari *et al.* 2014), the imported ice volume from the Arctic Basin (e.g. Kwok 2009), and other meteorological and hydrological conditions (Loeng 1991; Sundfjord *et al.* 2007).

However, few studies have focused on the climatic features on ice velocity and thickness conditions of the offshore drift ice in the Barents Sea. Unlike the fast ice along the

shoreline, the drift ice is often driven by the wind and sea current. According to the buoy observations, the drift ice velocity near the Svalbard was about 20 cm s^{-1} (Vinje & Kvambekk 1991). Other investigations are mainly concerned with the tracking of icebergs. Løset & Carstens (1996) introduced the sea ice and iceberg observation program in the western Barents Sea in 1987. In May 2003, some icebergs were observed with a mean speed of 14 cm s^{-1} in a direction of 228° in the northern Barents Sea (Zubakin *et al.* 2005) and the fastest recorded value was 24 cm s^{-1} (Dmitriyev *et al.* 2005). Based on the buoy measurements in spring 2004, the maximum ice motions near the Novaya Zemlya were between 39.7 and 48.9 cm s^{-1} (Dmitriyev *et al.* 2005). As for the ice thickness, the fast ice along the coastline rather than offshore drift ice has been studied. Gerland *et al.* (2008) presented the fast ice thickness variations at Hopen Island during 1966–2007, revealing that the maximum thickness was in May

with 99 cm on average. This is also the longest observed data in the Barents Sea. Forsström *et al.* (2011) collected some scattered 44-points thickness measurements of drift ice and fast ice based on drillings in the marginal ice zone of Barents Sea during 1999–2008. Recently, King *et al.* (2017) published two new ice helicopter-borne-electromagnetic thickness measurements in March 2003 and 2004 in the northwestern Barents Sea, showing the modal sea ice thickness varying regionally from 60 to 140 cm.

It must be noted that the available observed drift ice data are mainly short-term temporally and scattered spatially in the aforementioned studies. However, there are scarce long-term consecutive and direct drift ice measurements in Arctic regions, largely on account of the block of higher-concentration sea ice. Thus, satellite and reanalysis data can perhaps serve as an effective alternative. Among the satellite retrieval data products, the gridded sea ice motion dataset in the Polar Pathfinder Daily 25 km EASE-Grid Sea Ice Motion Vectors from National Snow and Ice Data Center (NSIDC) has been widely used. Various researchers have adopted the dataset to study the variability of Arctic sea ice speeds (Olason & Notz 2014; Sumata *et al.* 2015), tracking Arctic drift ice trajectory (Tschudi *et al.* 2010), the interaction between ice motion and external atmospheric forcing, such as the cyclonic and anti-cyclonic controls (Tsukernik *et al.* 2010; Scoccimarro *et al.* 2012). Regarding the ice thickness, the Climate Forecast System Reanalysis (CFSR) dataset (Saha *et al.* 2010) and the Climate Forecast System Version 2 (CFSv2) (Saha *et al.* 2011) from the National Centers for Environmental Prediction (NCEP) can provide continuous long-term ice thickness data. In detail, the reanalysis product is a complete integration and assimilation of both observed and modeled sea ice.

This paper attempts to characterize and describe the long-term offshore drift ice climatic behaviors in the northern Barents Sea from 1987 to 2016 using the ice motion datasets from NSIDC and ice thickness datasets from NECP-CFSR and CFSv2. The data description and study locations are described below in Materials and methods. Then the climatic ice features, including ice speed roses, ice thickness frequency distributions, and annual maximum values, are shown in the Results and discussion section. Finally, some relevant conclusions are given.

MATERIALS AND METHODS

Data description

The sea ice movement vectors were available from the Polar Pathfinder Daily 25 km EASE-Grid Sea Ice Motion Vectors dataset from NSIDC for the period from 1987 to 2016 (Tschudi *et al.* 2016). The ice drift velocity fields were derived using the images from the passive microwave observations based on satellite sensors and processed in the Northern Hemisphere EASE-Grids projection with a grid cell size of 25×25 km. In the following calculation, the ice motion data has been divided by 10 to revert to original units (cm s^{-1}). This ice motion dataset has been adopted to quantify the ice motion patterns in the Arctic as described in the preceding section.

The sea ice thickness data were obtained from the NECP-CFSR from 1987 to 2010 and NECP-CFSv2 dataset from 2011 to 2016 (Saha *et al.* 2010, 2011). In temporal resolution, both the datasets offer the thickness data four times per day, namely, 0, 6, 12 and 18 h. In spatial resolution, the CFSR is approximately $0.312 \times 0.312^\circ$ while the CFSv2 is $0.205 \times 0.204^\circ$. The sea ice model used in this reanalysis was blended with an assimilation processing and modifications system. Specifically, the sea ice dynamic sub-model adopts the elastic-viscous-plastic approach (Hunke & Dukowicz 1997) and the thermodynamic sub-model utilizes the nonlinear process parameterization (Winton 2000) with five sea ice thickness classifications (Saha *et al.* 2010).

Representative study sites

In terms of the sea ice concentrations obtained from the NSIDC (Cavalieri *et al.* 1996), the sea ice distribution in the Barents Sea advances southwards to its highest peak in April while it recedes northwards to the lowest trough in September. This result is consistent with the conclusions in previous studies (Kwok 2009; Duan *et al.* 2018). The two corresponding isoplethes of sea ice edge are illustrated in Figure 1, portrayed by solid and dotted curves. Consequently, the ice cover undergoes a seasonal extension and retreat between the two ice edge lines. In view of this periodic variation, three fixed points labeled P1 to P3 were selected (Figure 1) in order to obtain an insight into the drift ice climatology characteristics. The P1, P2 and P3 lie

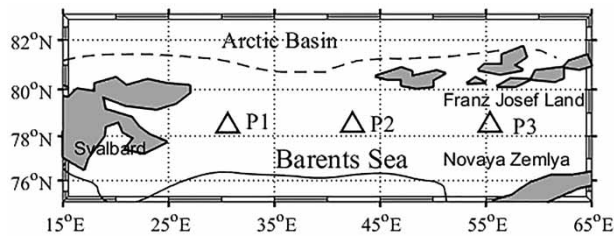


Figure 1 | Geographical map of northern Barents Sea and locations chosen for further drift ice climatic characteristics analysis.

in the western, central and eastern regions, respectively. The bilinear interpolation approach was chosen to obtain the ice velocity and thickness data series at the three locations.

RESULTS AND DISCUSSION

Climatologic velocity characteristics of drift ice

Annual ice rose diagram analysis

Like the wind and wave roses, in order to gain a better understanding of climatic drift ice behaviors it is important

to study the drift ice direction and speed proportional distributions. In this regard, the drift ice rose diagrams were calculated at the three locations. Herein, the ice motion direction is defined as the direction which it flows towards. For instance, a northerly drift ice flows from the south to the north and has an ice direction of 0° , and so forth.

Based on the 30-year ice motion dataset, [Figure 2](#) illustrates the annual ice roses from P1 to P3. Overall, the directions from WSW to SE are common in the three sites. Specifically, at P1 S occurs predominantly, which exceeds 10%; at P3 SW is more dominant, exceeding 10% as well, and SSW is also more prevailing; at P2 SSE is relatively prevalent though the directions from SW to SE seem somewhat evenly distributed. Besides, the ice speed was classified into six levels from 0 to $>30 \text{ cm s}^{-1}$ with the interval of 5 or 10 cm s^{-1} (see the legend in [Figure 2](#)). At P1 lower speeds of less than 10 cm s^{-1} are more common; at P2 and P3 higher speeds exceeding 15 cm s^{-1} occur more frequently. It should be noted that in [Figure 2](#) the percentages in the central part of the ice roses represent the

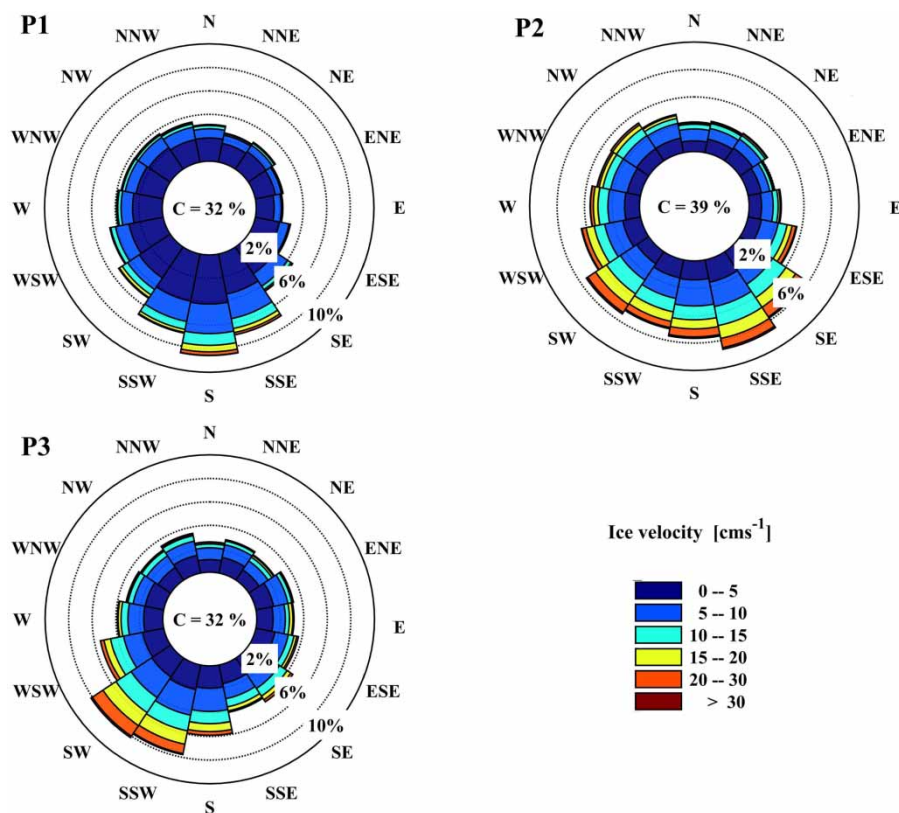


Figure 2 | Annual drift ice rose diagrams from P1 to P3.

frequency of ice-free state and ice-static state. According to the percentages, it can be inferred that there are approximately four months with ice-free conditions in the selected points throughout the year.

Monthly ice rose diagram analysis

The drift ice directions are also closely dependent on the weather conditions, in particular, the strong synoptic process. In other words, the ice motion directions change

yearly, seasonally, monthly or even daily. Therefore, monthly ice rose analysis is an indispensable content to comprehend the temporal variations. Figures 3–5 show the monthly ice roses at the three locations.

In Figures 3–5, the ice roses in the summer months (i.e. July–October) are not shown because the high-concentration sea ice is unlikely to form in these periods. From Figure 3, at P1 the S is of great predominance in January, March, April and May, even exceeding 18%. The SSW and SSE are relatively prevalent in February and June,

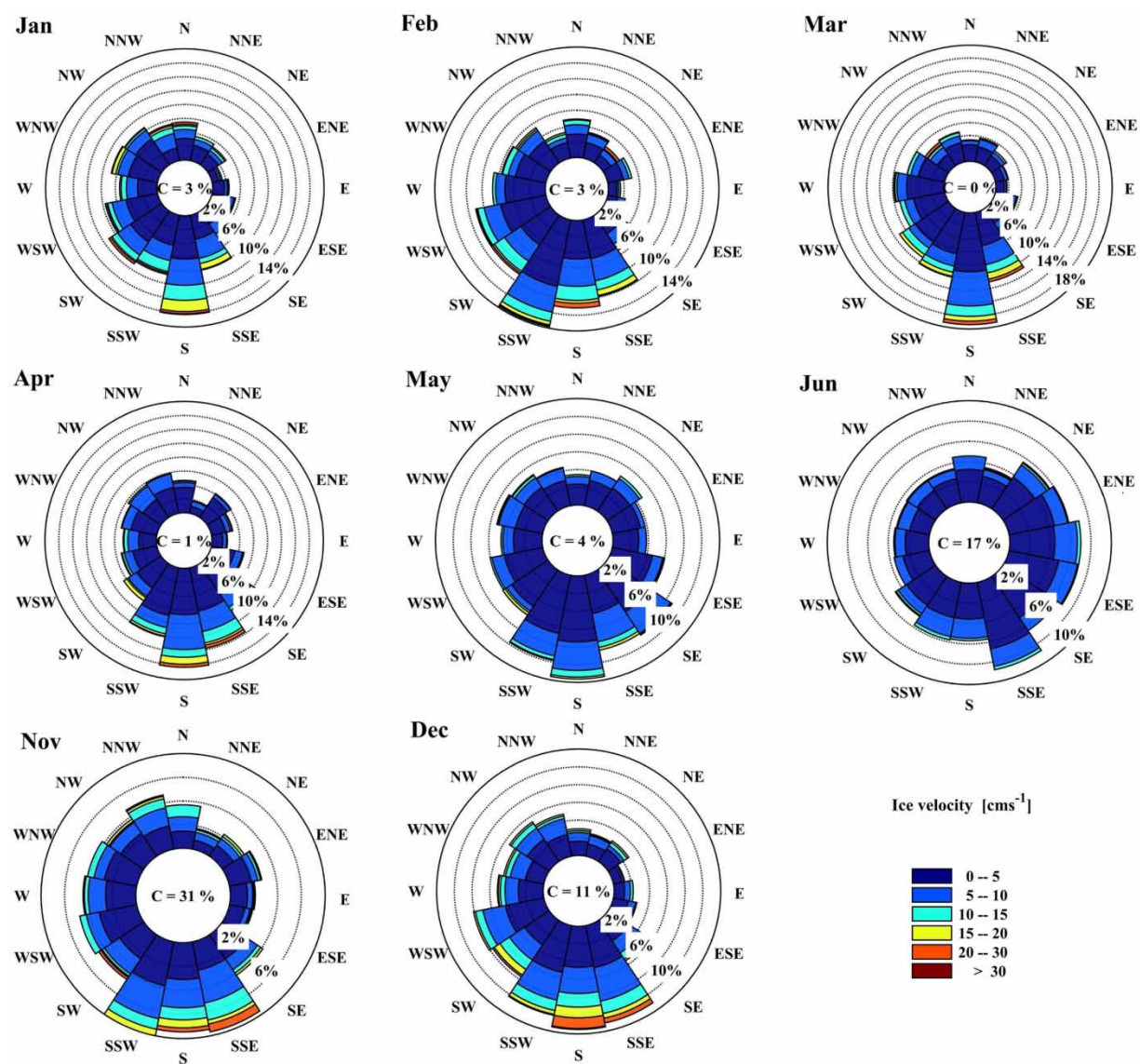


Figure 3 | Monthly drift ice rose diagrams at P1.

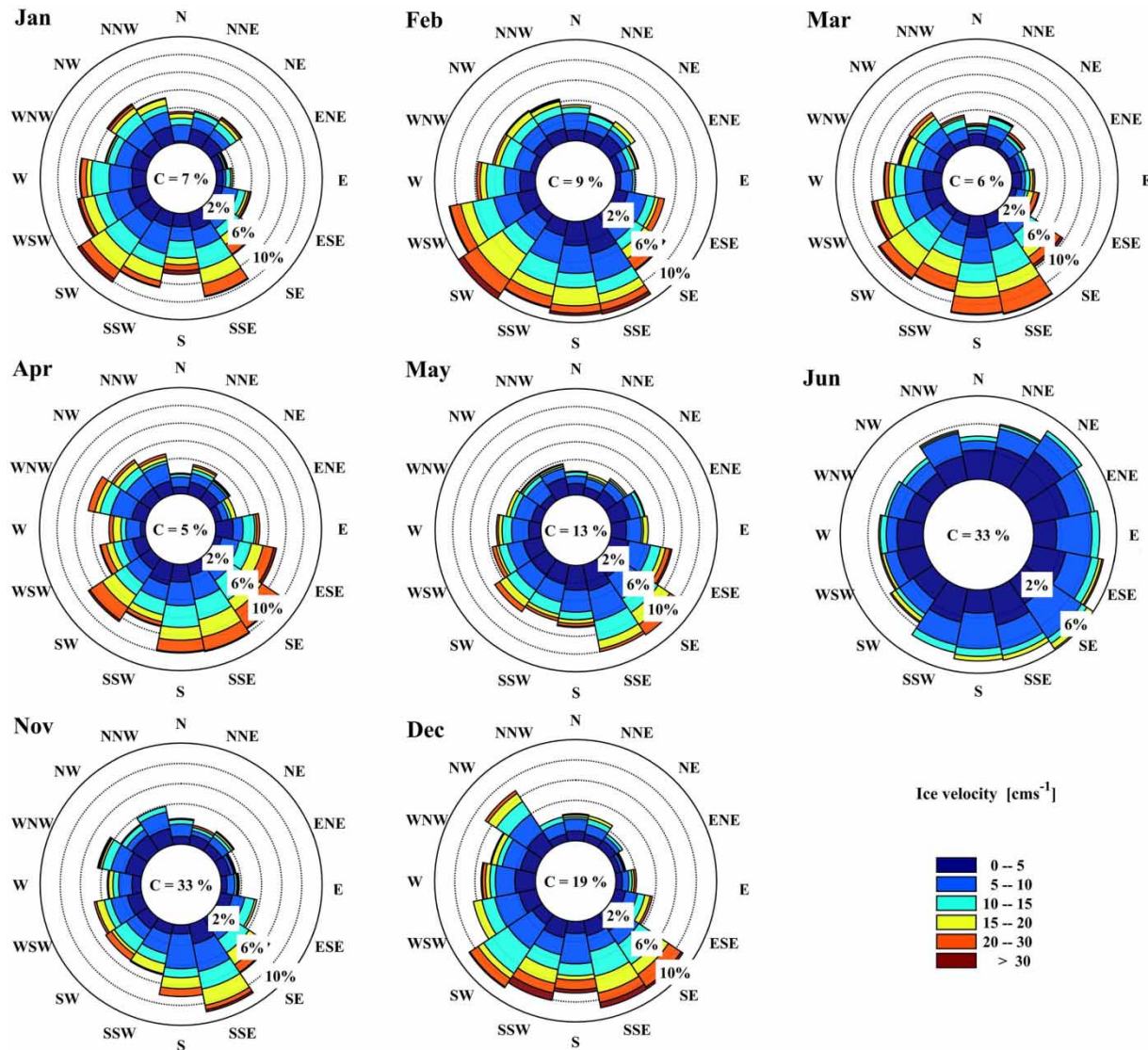


Figure 4 | Monthly drift ice rose diagrams at P2.

respectively. In November and December, directions from SSW to SSE are more frequent. The ice speeds higher than 15 cm s^{-1} mainly appear from November to April. Things are different in P2 and P3. From [Figure 4](#), at P2 directions from WSW to SE are recurrent from December to April. In November and May, the SSE and SE are comparatively dominant. Besides, all the directions are no more than 10% in each month. From [Figure 5](#), at P3 SW and SSW appear more commonly in each month except in June. Further, in general the higher speeds occur in each month for both P2 and P3 while June is the calmest month.

However, at P1, the larger speeds primarily appear in November and December.

Maximum ice speed rose diagram analysis

The maximum ice speed rose diagrams, representing the ice speed maxima at each direction during the 30 years, have been computed. As shown in [Figure 6](#), the maximum ice speed can be up to more than 40 cm s^{-1} in some directions, which is approximately equivalent to the ice speeds near the Novaya Zemlya ([Dmitriyev et al. 2005](#)). At P1 most

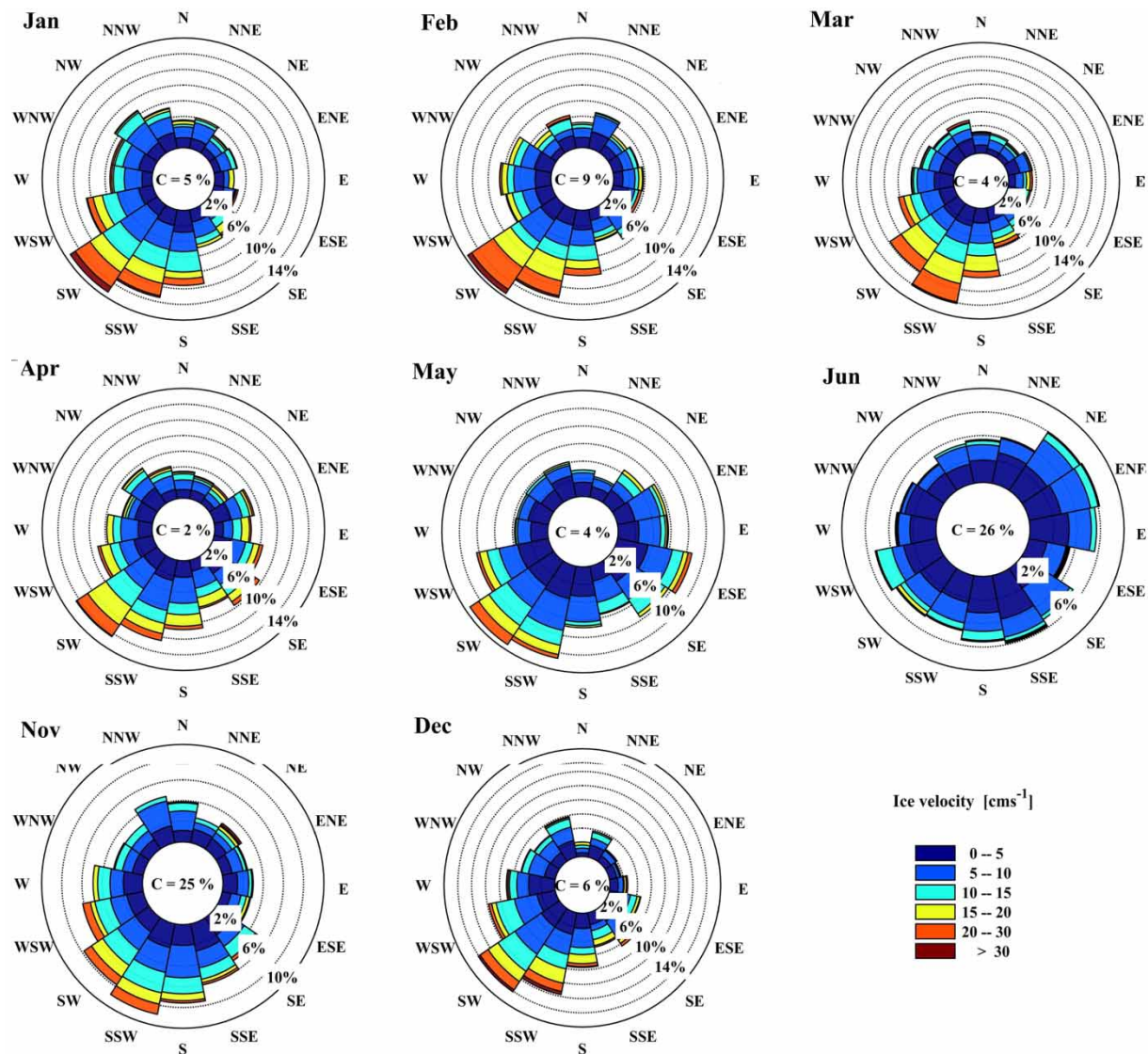


Figure 5 | Monthly drift ice rose diagrams at P3.

directions are with ice speed maxima between 20 and 30 cm s^{-1} ; the NW, W, SSW and SSE are between 20 and 30 cm s^{-1} ; and S is the largest ice speed at 40.5 cm s^{-1} . P3 is similar to P1 in ice speed magnitude. From NW to SE, the ice speed maxima are primarily between 20 and 30 cm s^{-1} ; the WNW, WSW, S and SSE are between 20 and 30 cm s^{-1} ; and the largest ice speed is 43.2 cm s^{-1} at SW direction. At P3 the ice speed maxima are larger than that at each direction in P1 and P3. From WSW to SE, the ice speed maxima are mainly at a range between 40 and 50 cm s^{-1} with the largest speed of 45.9 cm s^{-1} at SW

direction. Combined with the monthly ice rose analysis, one can conclude that prevailing ice directions coincide well with strong ice directions.

Interannual variability of maximum ice speed conditions

Making clear the interannual variability of ice speed conditions is also required in order to obtain more detailed climatologic drift ice characteristics. Hence, temporal variations of annual maximum ice speeds combined with its

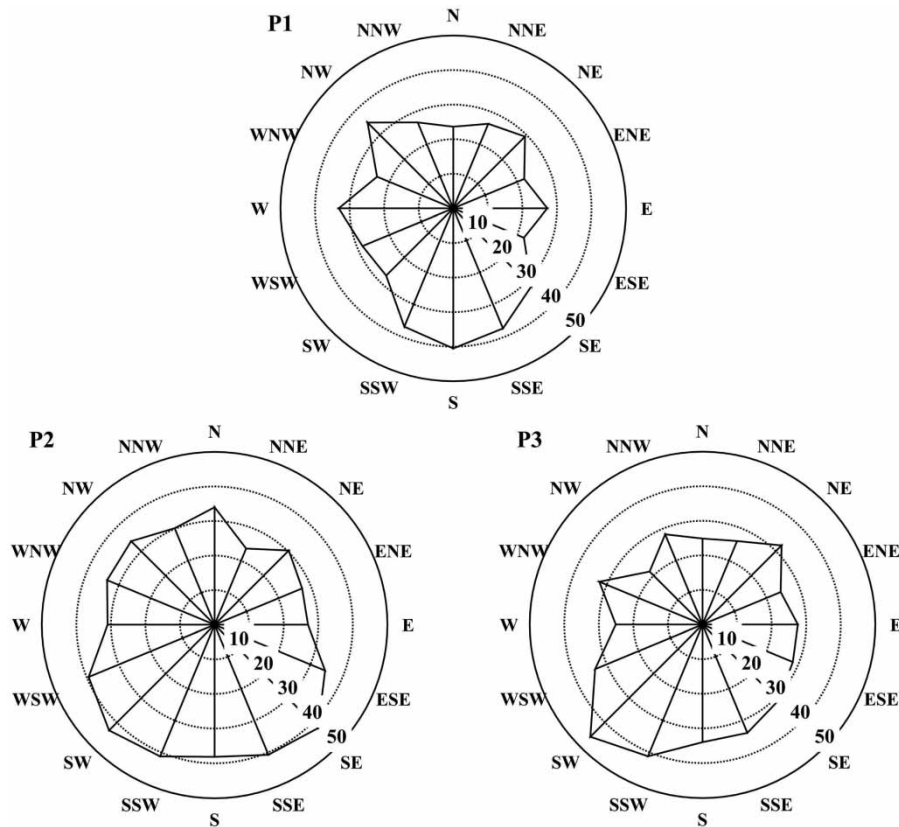


Figure 6 | Maximum ice speed rose diagrams analysis from P1 to P3.

simultaneous direction and occurrence moment at the three locations from 1987 to 2016 have been continuously analyzed and illustrated in [Figures 7–9](#).

As is seen in [Figure 7](#), the annual maximum ice speed sequences of the three selected sites are approximately in the range of $15\text{--}45\text{ cm s}^{-1}$. Meanwhile, the annual maximum speed series at P2, where almost all years have values $>30\text{ cm s}^{-1}$, is relatively larger than that at P1 and P3. Specially, at P1 the largest ice speed peak is 40.5 cm s^{-1} in 2014; at P2 the largest peak is 43.2 cm s^{-1} in 2006 but with larger peaks in 1992, 1993, 1995, 2002, 2009 and 2014 as well; at P3 the largest peak is 45.9 cm s^{-1} in 2002 with the second largest in 1999.

Regarding the synchronous directions, an obvious generality can be inferred from [Figure 8](#). The overwhelming majority of the directions occur between 135° (90° for P2) and 270° , except for the occasional leaps such as at P1 in 2015, at P2 in 1988 and 2015, and at P3 in 1989 and 2007. In other words, these directions are primarily

from W to SE. This conclusion is also in good agreement with the prevailing and strong ice speed directions in the rose analysis. As for the simultaneous occurrence moments, as is shown in [Figure 9](#), the moments are fundamentally uniformly distributed in winter months from November to April. Abnormal conditions rarely occur in other months.

Climatologic thickness characteristics of drift ice

Probability distribution of ice thickness frequency

By analyzing the 30-year ice thickness datasets from CFSR and CFSv2, the successive series of the drift ice thickness at the three sites were obtained. [Figure 10](#) illustrates the frequency distribution histograms of the ice thickness with an interval of 10 cm.

From [Figure 10](#), the drift ice thickness is primarily distributed from 0 to 180 cm. Specifically, the ice thickness is

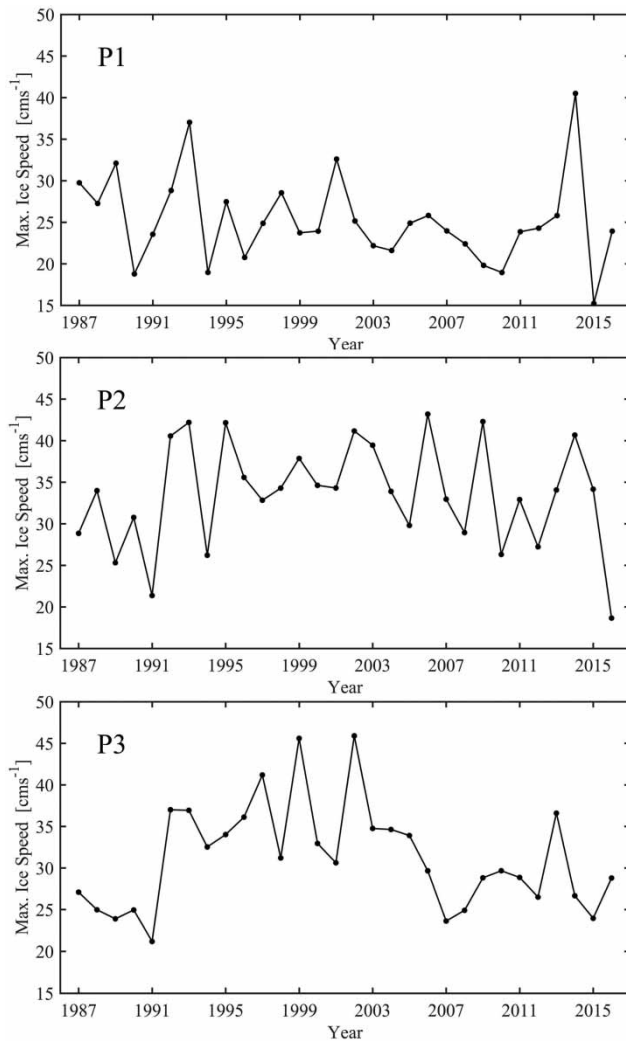


Figure 7 | Interannual variability of annual maximum ice speed from P1 to P3 during 1987–2016.

overwhelmingly distributed in two spectacular intervals, namely, a thicker interval between 70 and 120 cm (130 cm for P3), and a thinner interval of between 20 and 70 cm. In particular, there is an extraordinarily largest-frequency thickness peak at P3, which is between 110 and 120 cm, accounting for 20% of the total. However, for P1 and P2 the largest-frequency peak is between 80 and 90 cm, which is obviously lower than the corresponding peak at P3. The ice thickness greater than 150 cm is in the lowest occurrence frequency. Regarding the multiyear average ice thickness, the three locations are at 57, 55 and 66 cm, respectively, while for the median thickness, they are at 72, 70 and 83 cm,

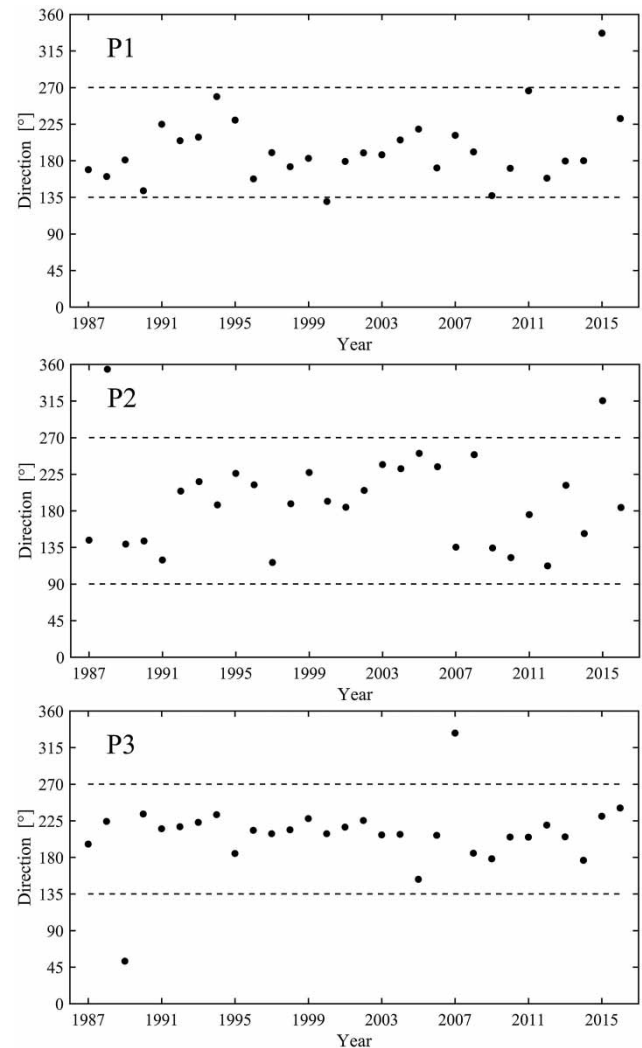


Figure 8 | Interannual variability of simultaneous directions of annual maximum ice speed from P1 to P3 during 1987–2016.

respectively. A comparison between average and median thickness also indicates that the probability distribution of ice thickness is apparently in negative skewness at the three locations.

Interannual variability of maximum drift ice thickness conditions

Determining the interannual variations of annual maximum ice thickness is also essential to achieve more elaborate drift ice behaviors. Therefore, interannual variations of annual ice thickness maxima combined with its simultaneous occurrence moment at the three locations from 1987 to

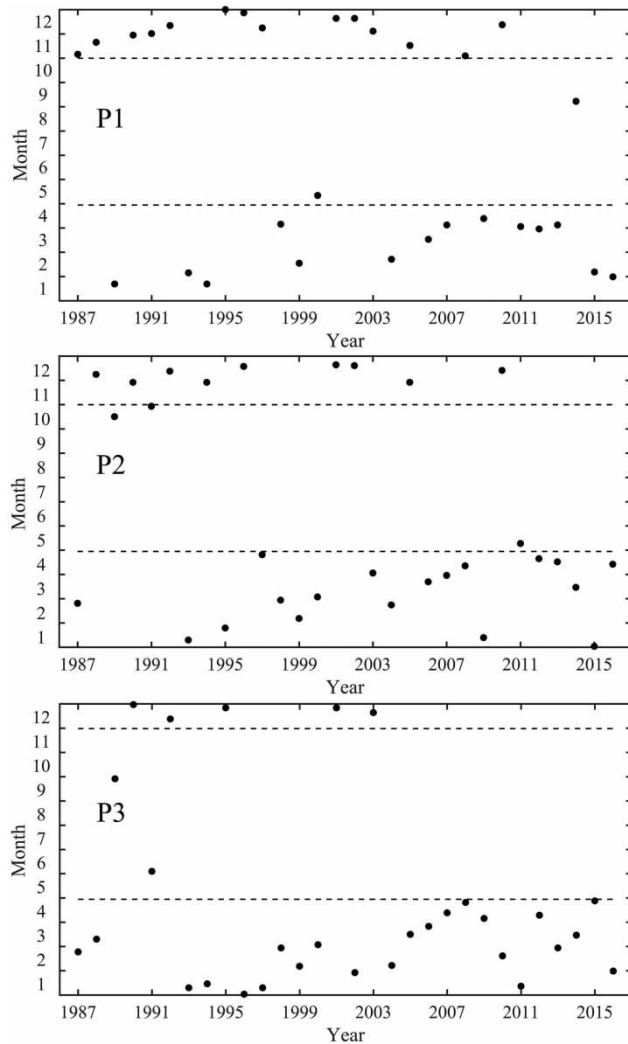


Figure 9 | Interannual variability of simultaneous occurrence moments of annual maximum ice speed from P1 to P3 during 1987–2016.

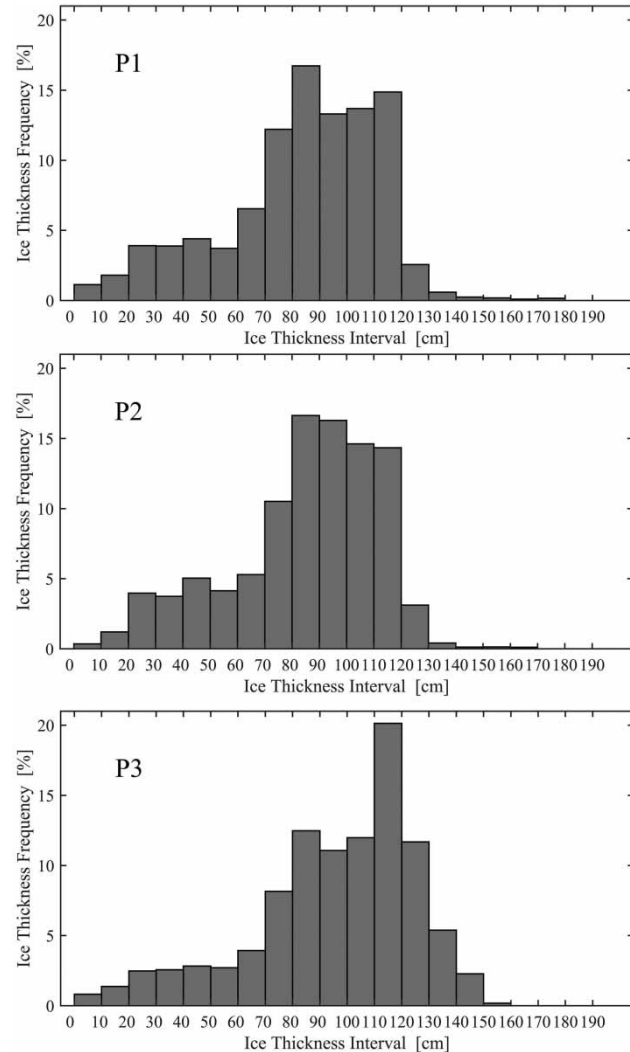


Figure 10 | Histograms of probability distribution frequency for ice thickness from P1 to P3.

2016 have been continuously calculated and illustrated in Figures 11 and 12.

From Figure 11, the annual maximum ice thickness series at the three chosen locations vary highly interannually with an approximate range between 90 and 170 cm. At P1 the largest ice thickness peak was 181 cm in 1995 with the second thickest (158 cm) in 2005; at P2 the largest peak was 164 cm in 1995; at P3 the largest peak was 151 cm in 2002. In addition, linear regression analysis exhibits a long-term negative trend of 7.1, 5.5 and 8.4 cm per decade (statistically significant at 0.1 level) at P1, P2 and P3, continuously from

1987 to 2016. This maximum thickness decreasing trend is roughly similar to the coastal fast ice at Hopen declining at 9.8 cm per decade (Gerland *et al.* 2008).

With regards to the simultaneous occurrence moments, a noticeable pattern can be found from Figure 12. At P1, the moments mainly appear from May to June and from November to January; at P2 and P3, the moments are mainly from April to May and from November to January. Compared to the analysis of ice velocity, the occurrence moments of annual ice thickness maxima are slightly different to those of ice speed maxima.

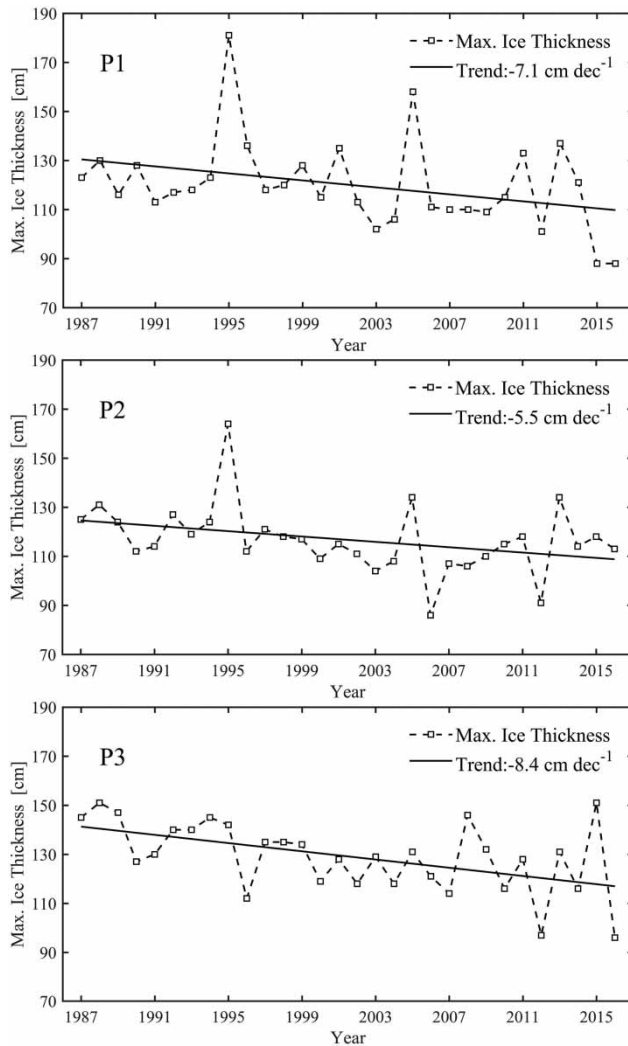


Figure 11 | Interannual variability and trends of annual maximum ice thickness from P1 to P3.

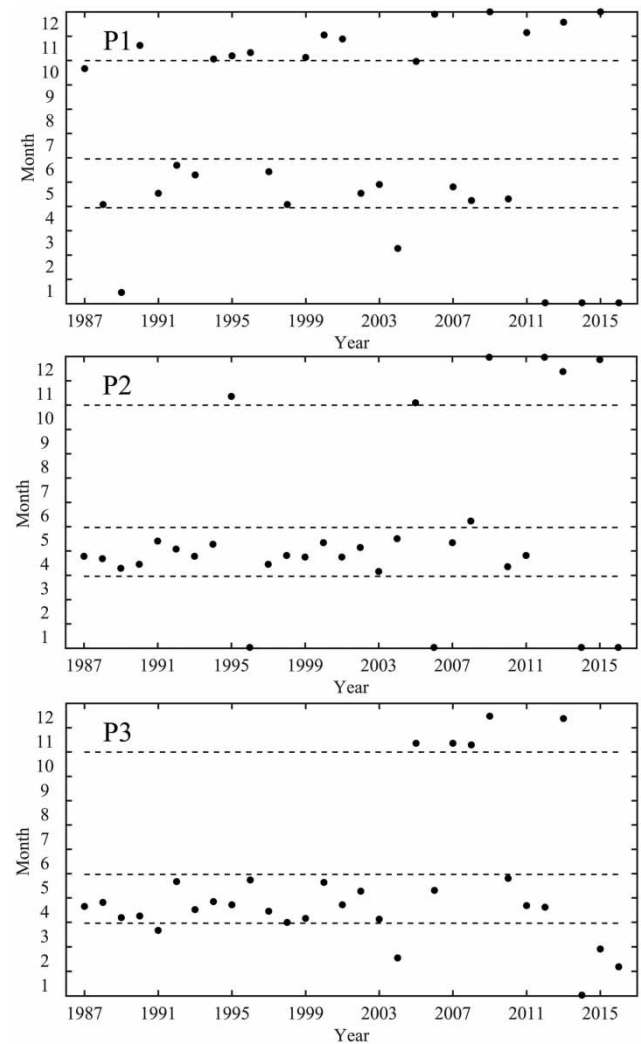


Figure 12 | Interannual variability of simultaneous occurrence moments of annual maximum ice thickness from P1 to P3.

CONCLUSIONS

Compared to previous studies regarding the sea ice concentration and its relationship with the governing dynamic and thermodynamic factors, this investigation has focused on the offshore drift ice in the northern Barents Sea and presented a preliminary statistical description of climatic characteristics of drift ice velocity and thickness.

Three typical locations have been selected in order to obtain a detailed analysis. Annual and monthly drift ice roses indicate that the directions from WSW to SE are primarily prevailing, in particular in winter months, at the

three sites. The higher speeds above 30 cm s^{-1} occurred in each direction and speeds greater than 40 cm s^{-1} appeared in some southerly directions. Both the annual maximum ice speed and thickness series vary obviously interannually. For ice speed, the annual speed maxima are mainly between 15 and 45 cm s^{-1} occurring in the southerly directions from November to April. For the ice thickness, it is overwhelmingly distributed in a thicker interval between 70 and 120 cm (130 cm for P3), and a thinner interval between 20 and 70 cm . The annual thickness maxima approximately range from 90 to 170 cm , occurring from May to June and from November to January.

In summary, this study promotes the understanding of climatic drift ice conditions in the northern Barents Sea from 1987 to 2016 based on satellite datasets from NSIDC and reanalysis datasets from NECP-CFSR and CFSv2. However, further research is still required to reduce the uncertainty if more direct observed high-resolution datasets are available.

ACKNOWLEDGEMENTS

The authors are grateful to the anonymous reviewer for valuable suggestions that helped to improve this paper. This work was financially supported by the National Natural Science Foundation of China (Nos. 51779236 and 51509226).

REFERENCES

- Cavalieri, D. J., Parkinson, C. L., Gloersen, P. & Zwally, H. J. 1996 *Updated Yearly Sea Ice Concentrations From Nimbus-7 SMMR and DMSP SSM/I-SSMIS Passive Microwave Data, Version 1*. NASA National Snow and Ice Data Center Distributed Active Archive Center, Boulder, Colorado, USA.
- Dmitriyev, N. Y., Voinov, G. N., Gudoshnikov, Y. P., Nesterov, A. V. & Skutin, A. A. 2005 Study of the dynamics of icebergs of the Barents Sea. In: *Proc. 18th Int. Conf. on Port and Ocean Eng. Under Arctic Conditions*, Vol. 2. Potsdam, New York, USA, pp. 521–530.
- Duan, C. L., Wang, Z. F. & Dong, S. 2018 Wave characteristics and wave energy assessment in the Barents Sea. *Pol. Polar Res.* **39** (1), 145–164.
- Forsström, S., Gerland, S. & Pedersen, C. A. 2011 Thickness and density of snow-covered sea ice and hydrostatic equilibrium assumption from in situ measurements in Fram Strait, the Barents Sea and the Svalbard coast. *Ann. Glaciol.* **52** (57), 261–270.
- Gerland, S., Renner, A. H. H., Godtliessen, F., Divine, D. & Løyning, T. B. 2008 Decrease of sea ice thickness at Hopen, Barents Sea, during 1966–2007. *Geophys. Res. Lett.* **35**, L06501.
- Hunke, E. C. & Dukowicz, J. K. 1997 An elastic–viscous–plastic model for sea ice dynamics. *J. Phys. Oceanogr.* **27** (9), 1849–1867.
- Kern, S., Kaleschke, L. & Spreen, G. 2010 Climatology of the Nordic (Irminger, Greenland, Barents, Kara and White/Pechora) Seas ice cover based on 85 GHz satellite microwave radiometry: 1992–2008. *Tellus. A.* **62** (4), 411–434.
- King, J., Spreen, G., Gerland, S., Haas, C., Hendricks, S., Kaleschke, L. & Wang, C. 2017 Sea-ice thickness from field measurements in the northwestern Barents Sea. *J. Geophys. Res. Oceans* **122** (2), 1497–1512.
- Kwok, R. 2009 Outflow of Arctic Ocean sea ice into the Greenland and Barents Seas: 1979–2007. *J. Clim.* **22** (9), 2438–2457.
- Loeng, H. 1991 Features of the physical oceanographic conditions of the Barents Sea. *Polar Res.* **10** (1), 5–18.
- Løset, S. & Carstens, T. 1996 Sea ice and iceberg observations in the western Barents Sea in 1987. *Cold Reg. Sci. Technol.* **24** (4), 323–340.
- Nakanowatari, T., Sato, K. & Inoue, J. 2014 Predictability of the Barents Sea ice in early winter: remote effects of oceanic and atmospheric thermal conditions from the North Atlantic. *J. Clim.* **27** (23), 8884–8901.
- Olason, E. & Notz, D. 2014 Drivers of variability in Arctic sea-ice drift speed. *J. Geophys. Res. Oceans* **119** (9), 5755–5775.
- Saha, S., Moorthi, S., Pan, H. L., Wu, X., Wang, J., Nadiga, S., Tripp, P., Kistler, R., Woollen, J., Behringer, D., Liu, H., Stokes, D., Grumbine, R., Gayno, G., Wang, J., Hou, Y., Chuang, H., Juang, H. H., Sela, J., Iredell, M., Treadon, R., Kleist, D., Delst, P. V., Derber, J., Ek, M., Meng, J., Wei, H., Yang, R., Lord, S., Dool, H. V. D., Kumar, A., Wang, W., Long, C., Chelliah, M., Xue, Y., Huang, B., Schemm, J., Ebisuzaki, W., Lin, R., Xie, P., Chen, M., Zhou, S., Higgins, W., Zou, C., Liu, Q., Chen, Y., Han, Y., Cucurull, L., Reynolds, R. W., Rutledge, G. & Liu, H. 2010 *NCEP Climate Forecast System Reanalysis (CFSR) 6-Hourly Products, January 1979 to December 2010*.
- Research Data Archive at the National Center for Atmospheric Research, Computational and Information Systems Laboratory, Boulder, Colorado, USA.
- Saha, S., Moorthi, S., Wu, X., Wang, J., Nadiga, S., Tripp, P., Behringer, D., Hou, Y., Chuang, H., Iredell, M., Ek, M., Meng, J., Yang, R., Mensez, M. P., Dool, H. V. D., Zhang, Q., Wang, W., Chen, M. & Ek, M. 2011 *NCEP Climate Forecast System Version 2 (CFSv2) 6-Hourly Products (Updated Daily)*. Research Data Archive at the National Center for Atmospheric Research, Computational and Information Systems Laboratory, Boulder, Colorado, USA.
- Scoccimarro, E., Gualdi, S. & Navarra, A. 2012 Tropical cyclone effects on Arctic Sea ice variability. *Geophys. Res. Lett.* **39** (17), L17704.
- Sorteberg, A. & Kvindedal, B. 2006 Atmospheric forcing on the Barents Sea winter ice extent. *J. Clim.* **19** (19), 4772–4784.
- Sumata, H., Gerdes, R., Kauker, F. & Karcher, M. 2015 Empirical error functions for monthly mean Arctic sea-ice drift. *J. Geophys. Res. Oceans* **120** (11), 7450–7475.
- Sundfjord, A., Fer, I., Kasajima, Y. & Svendsen, H. 2007 Observations of turbulent mixing and hydrography in the marginal ice zone of the Barents Sea. *J. Geophys. Res. Oceans* **112** (C5), C05008.
- Tschudi, M., Fowler, C., Maslanik, J. & Stroeve, J. 2010 Tracking the movement and changing surface characteristics of Arctic sea ice. *IEEE J-Stars* **3** (4), 536–540.
- Tschudi, M., Fowler, C., Maslanik, J., Stewart, J. S. & Meier, W. 2016 *Polar Pathfinder Daily 25 km EASE-Grid Sea Ice*

- Motion Vectors, Version 3*. NASA National Snow and Ice Data Center Distributed Active Archive Center, Boulder, Colorado, USA.
- Tsukernik, M., Deser, C., Alexander, M. & Tomas, R. 2010 [Atmospheric forcing of Fram Strait sea ice export: a closer look](#). *Clim. Dynam.* **35** (7–8), 1349–1360.
- Vinje, T. & Kvambekk, Å. S. 1991 [Barents Sea drift ice characteristics](#). *Polar Res.* **10** (1), 59–68.
- Winton, M. 2000 [A reformulated three-layer sea ice model](#). *J. Atmos. Ocean Tech.* **17** (4), 525–531.
- Zubakin, G. K., Shelomentsev, A. G., Onshuus, D. K., Eide, L. I. & Buzin, I. V. 2005 Spatial distribution of icebergs in the Barents Sea based on archived data and observations of 2003. In: *Proc. 18th Int. Conf. on Port and Ocean Eng. Under Arctic Conditions*, Vol. 2. Potsdam, New York, USA, pp. 575–584.

First received 28 September 2018; accepted in revised form 21 February 2019. Available online 25 March 2019